Earth Abundant Fe/Mn-Based Layered Oxide Interconnected Nanowires for Advanced K-Ion Full Batteries

Xuanpeng Wang, Xiaoming Xu, Chaojiang Niu,* Jiashen Meng, Meng Huang, Xiong Liu, Ziang Liu, and Liqiang Mai*

State Key Laboratory of Advanced Technology for Materials Synthesis and Processing, International School of Materials Science and Engineering, Wuhan University of Technology, Wuhan 430070, China

S *Supporting Information*

ABSTRACT: K-ion battery (KIB) is a new-type energy storage device that possesses potential advantages of low-cost and abundant resource of K precursor materials. However, the main challenge lies on the lack of stable materials to accommodate the intercalation of large-size K-ions. Here we designed and constructed a novel earth abundant Fe/Mn-based layered oxide interconnected nanowires as a cathode in KIBs for the first time, which exhibits both high capacity and good cycling stability. On the basis of advanced in situ X-ray diffraction analysis and electrochemical characterization, we confirm that interconnected $K_{0.7}Fe_{0.5}Mn_{0.5}O_2$ nanowires can provide stable framework structure, fast K-ion diffusion channels, and three-dimensional electron transport network during the depotassiation/potassiation processes. As a result, a considerable initial discharge capacity of 178 mAh g^{-1} is achieved when measured for KIBs. Besides, K-ion full batteries based on interconnected $K_{0.7}Fe_{0.5}Mn_{0.5}O_2$ nanowires/soft carbon are assembled, manifesting over 250 cycles with a capacity retention of ~76%. This work may open up the investigation of high-performance K-ion intercalated earth abundant layered cathodes and will push the development of energy storage systems.

KEYWORDS: Interconnected nanowires, K-ion full batteries, Fe/Mn-based layered oxide, high-capacity, superior cycling stability, in situ X-ray diffraction
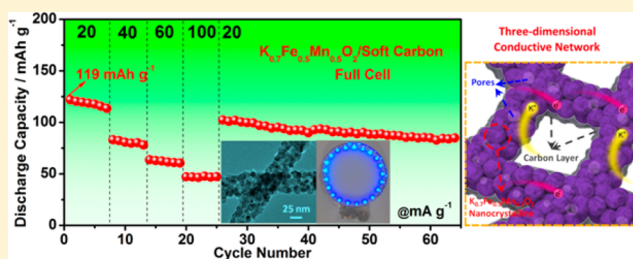
With the development of clean energy sources and the further promotion of smart grid, energy storage systems are critical for renewable integration of the energy infrastructure.[1−4] Among the various energy storage technologies, many types of rechargeable batteries have been developed, such as traditional lead-acid batteries, nickel−cadmium batteries, new-type lithium ion batteries, and so forth.[5,6] Each traditional battery has its own shortcomings and issues, so they can hardly meet the increasing demands for energy storage systems.[7−10] Additionally, the development of lithium ion batteries has encountered a big bottleneck, therefore developing new-type energy storage batteries is urgently desired.[11−13]

To the best of our knowledge, a variety of new-type energy storage batteries have been studied, such as Na-ion batteries, Mg-ion batteries, Zn-ion batteries, Ca-ion batteries, and mixed ions batteries.[2−4,8−10,14,15] Recently, a new concept of K-ion battery (KIB) has been reported based on the K-ion insertion/extraction mechanism, which originates from the abundance of K precursor materials in the Earth's crust (the reserve of K element is very close to Na) and similar output voltages to lithium ion batteries in theory.[16−26] However, due to the large size of K-ions, most of cathodes can hardly adapt to the structure degradation during depotassiation/potassiation processes, resulting in short-term cycling stability and low capacity. Prussian family materials with large diffusion channels lately

have been reported as cathodes in KIBs, while the low conductivity and poor cycling stability limit their potassium storage performances.[20,22] Therefore, it is highly desirable to seek a new KIBs cathode with a stable framework structure during the insertion/extraction processes of large-size K-ions.

Alkali metal ions (K^+, Na^+, Li^+) intercalated layered oxide cathode are widely studied due to their high theoretical capacities, earth abundant, and environmentally friendly for energy storage systems.[1,2,9,16,27] However, the radius of K-ion (1.37 Å) is much larger than that of Na-ion (0.99 Å), leading to the poor ion transport kinetics. Here, we found that a part of K-ions can be extracted from the $K_{0.7}Fe_{0.5}Mn_{0.5}O_2$ in the depotassiation process, and the skeleton structure of the material remains stable after being charged. Therefore, we hypothesize that $K_{0.7}Fe_{0.5}Mn_{0.5}O_2$ might be a candidate for KIBs. Furthermore, one-dimensional nanomaterials have been extensively proved to improve the electrochemical properties of electrode materials.[28−43]
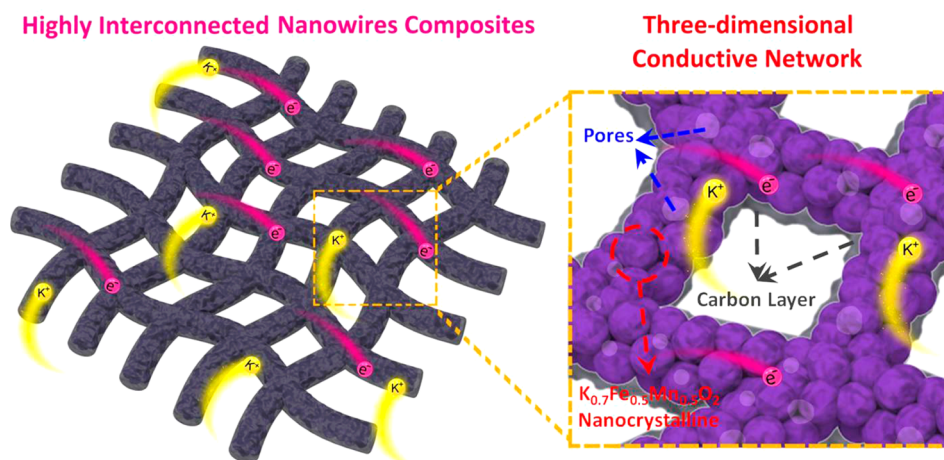
Herein, we designed and constructed a new-type earth abundant Fe/Mn-based layered oxide interconnected nanowires cathode in which $K_{0.7}Fe_{0.5}Mn_{0.5}O_2$ nanocrystals are
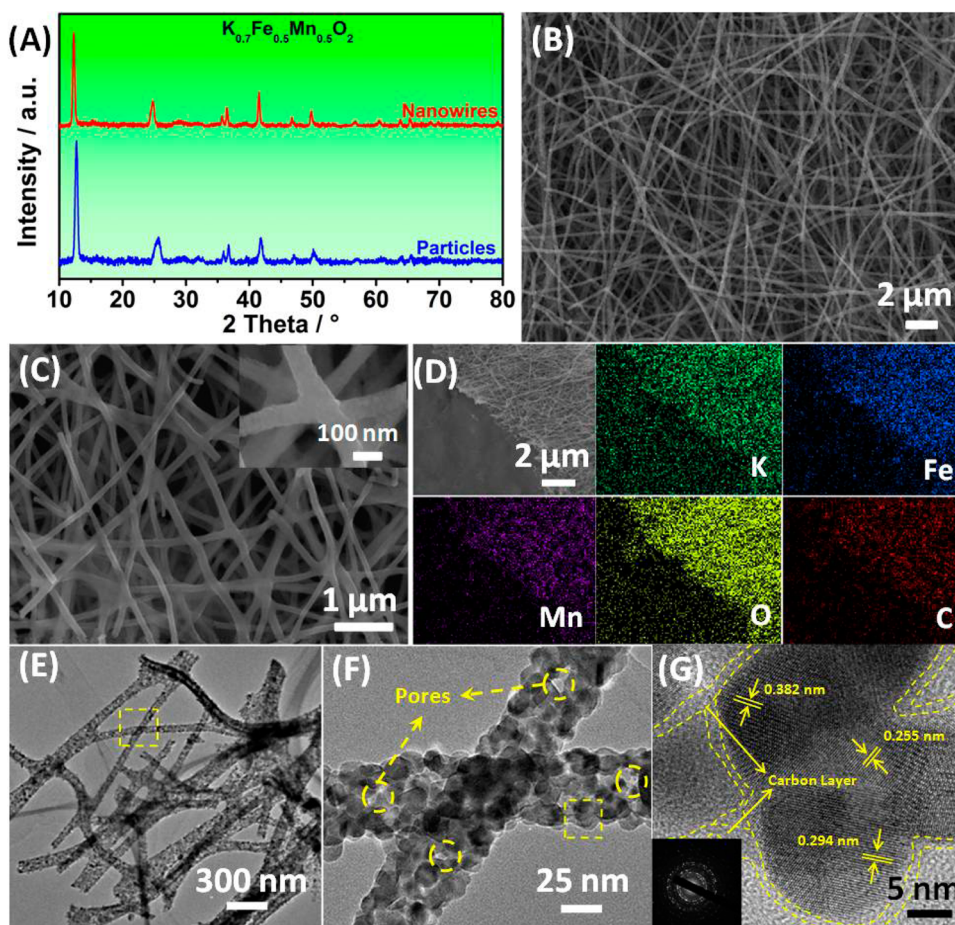
Figure 1. Schematic illustrations of the interconnected $K_{0.7}Fe_{0.5}Mn_{0.5}O_2$ nanowires with three-dimensional continuous electron/K-ion transport pathways and a large electrode−electrolyte contact area during the K-ion insertion/extraction processes.


Figure 2. (A) XRD patterns of interconnected $K_{0.7}Fe_{0.5}Mn_{0.5}O_2$ nanowires and $K_{0.7}Fe_{0.5}Mn_{0.5}O_2$ particles sintered at a temperature of 800 °C. SEM images (B,C) and EDS mapping images (D) of interconnected $K_{0.7}Fe_{0.5}Mn_{0.5}O_2$ nanowires. Inset of (C) is the SEM image of interconnected $K_{0.7}Fe_{0.5}Mn_{0.5}O_2$ nanowires. TEM images (E,F) and high-resolution TEM image (G) of interconnected $K_{0.7}Fe_{0.5}Mn_{0.5}O_2$ nanowires. Inset of (G) is the selected area electro diffraction (SAED) pattern of interconnected $K_{0.7}Fe_{0.5}Mn_{0.5}O_2$ nanowires.

uniformly encapsulated by carbon layers (Figure 1). Moreover, the advanced in situ X-ray diffraction (XRD) tests demonstrated that interconnected $K_{0.7}Fe_{0.5}Mn_{0.5}O_2$ nanowires can provide a stable crystal skeleton structure during the K-ion insertion/extraction processes. As a result, the interconnected $K_{0.7}Fe_{0.5}Mn_{0.5}O_2$ nanowires exhibit high discharge capacity and excellent cycling stability, when tested as a cathode in KIBs.

This work indicates an unexploited field of K-ion intercalated earth-abundant materials as a cathode for K-ion full batteries and may open up an entirely new avenue in the field of energy storage systems.

The formation process of interconnected $K_{0.7}Fe_{0.5}Mn_{0.5}O_2$ nanowires is illustrated in Figure S1. Both interconnected $K_{0.7}Fe_{0.5}Mn_{0.5}O_2$ nanowires and $K_{0.7}Fe_{0.5}Mn_{0.5}O_2$ particles
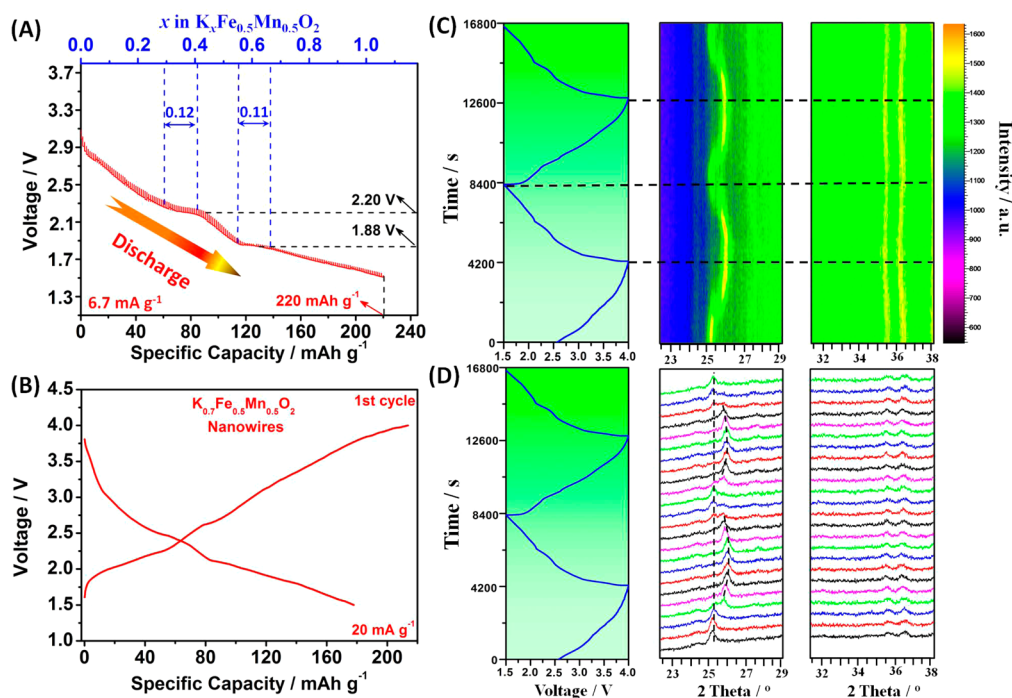
Figure 3. Potassium storage mechanism of the interconnected $K_{0.7}Fe_{0.5}Mn_{0.5}O_2$ nanowires. (A) The GITT test for interconnected $K_{0.7}Fe_{0.5}Mn_{0.5}O_2$ nanowires tested at a current density of 6.7 mA g^{-1} in a potassiation process. (B) The initial depotassiation/potassiation curves of interconnected $K_{0.7}Fe_{0.5}Mn_{0.5}O_2$ nanowires measured at 20 mA g^{-1}. (C) In situ XRD patterns of interconnected $K_{0.7}Fe_{0.5}Mn_{0.5}O_2$ nanowires during galvanostatic depotassiation/potassiation at 100 mA g^{-1}. The image plot of the XRD patterns at 22.5−29.0° and 31.5−38.0° during the first two cycles. (D) The image plot of the XRD patterns at 22.3−29.2° and 31.3−38.3° during the first two cycles.

exhibit highly crystalline phase (Figure 2A). The molar ratios of K/Fe/Mn are approximately 0.7:0.5:0.5 for both interconnected $K_{0.7}Fe_{0.5}Mn_{0.5}O_2$ nanowires and $K_{0.7}Fe_{0.5}Mn_{0.5}O_2$ particles (Table S1). When presintered at 300 °C, the corresponding XRD patterns reveal amorphous characteristics of both interconnected $K_{0.7}Fe_{0.5}Mn_{0.5}O_2$ nanowires and $K_{0.7}Fe_{0.5}Mn_{0.5}O_2$ particles (Figure S2). The morphology feature of interconnected $K_{0.7}Fe_{0.5}Mn_{0.5}O_2$ nanowires and $K_{0.7}Fe_{0.5}Mn_{0.5}O_2$ particles are presented in Figure S3. The diameters of the $K_{0.7}Fe_{0.5}Mn_{0.5}O_2$ nanowires are uniform (Figure 2B) and the nanowires are highly interconnected with each other (Figure 2C and inset of Figure 2C). Elemental mapping results demonstrate that all elements are uniformly distributed in interconnected $K_{0.7}Fe_{0.5}Mn_{0.5}O_2$ nanowires (Figure 2D).

The diameters of the individual nanowires are 50−150 nm (Figure 2E, F). Many particles are loaded in the nanowire (Figure 2F). High-resolution TEM (HRTEM) image of interconnected $K_{0.7}Fe_{0.5}Mn_{0.5}O_2$ nanowires displays clear lattice fringes, indicating high crystallinity (Figure 2G). The polycrystalline interconnected $K_{0.7}Fe_{0.5}Mn_{0.5}O_2$ nanowires are demonstrated in the Figure 2G inset. SEM images and elemental mapping of $K_{0.7}Fe_{0.5}Mn_{0.5}O_2$ particles are illustrated in Figure S4.

Thermogravimetric analysis (TGA) curves of interconnected $K_{0.7}Fe_{0.5}Mn_{0.5}O_2$ nanowires and $K_{0.7}Fe_{0.5}Mn_{0.5}O_2$ particles are shown in Figure S5A. The carbon contents of the two samples are determined to be ~4.8% and ~6.5%, respectively. Raman test results are shown in Figure S5B. For these two samples, the peak intensity of the G-band is comparable to that of the D-band, verifying the carbon is partially graphitized in these materials.[44−46] The pore structure of interconnected $K_{0.7}Fe_{0.5}Mn_{0.5}O_2$ nanowires and $K_{0.7}Fe_{0.5}Mn_{0.5}O_2$ particles

were measured by the Brunauer−Emmett−Teller (BET) and t-plot empirical law method. The interconnected $K_{0.7}Fe_{0.5}Mn_{0.5}O_2$ nanowires show an IV-type hysteresis loop (Figure S6). The specific surface area of interconnected $K_{0.7}Fe_{0.5}Mn_{0.5}O_2$ nanowires is calculated to be 23.0 m^2 g^{-1} (Figure S6A), which is 6.5 times higher than that of $K_{0.7}Fe_{0.5}Mn_{0.5}O_2$ particles (Figure S6C). For the interconnected $K_{0.7}Fe_{0.5}Mn_{0.5}O_2$ nanowires, the pore size is mainly centered at around 27 nm (Figure S6B). However, no pores exist in $K_{0.7}Fe_{0.5}Mn_{0.5}O_2$ particles as shown in Figure S6D.

To study the potassium storage mechanism of interconnected $K_{0.7}Fe_{0.5}Mn_{0.5}O_2$ nanowires in KIBs, the galvanostatic intermittent titration technique measurement (GITT) and in situ XRD experiment were conducted (Figure 3A−D). Before GITT test, the cell was charged to 4.0 V at 20 mA g^{-1}. The interconnected $K_{0.7}Fe_{0.5}Mn_{0.5}O_2$ nanowires display a theoretical discharge capacity of 220 mAh g^{-1} in GITT discharge test, corresponding to the insertion of ~1.06 K-ions per formula. Obviously, two discharge voltage plateaus are located at 2.20 and 1.88 V, which correspond to 0.12 and 0.11 K-ions insertion, respectively. When tested at a low current density of 20 mA g^{-1}, interconnected $K_{0.7}Fe_{0.5}Mn_{0.5}O_2$ nanowires exhibit high capacities of 214 and 178 mAh g^{-1} during the first depotassiation/potassiation processes, respectively (Figure 3B). The corresponding initial Coulombic efficiency is 83.2%.

The structural evolutions of the $K_{0.7}Fe_{0.5}Mn_{0.5}O_2$ during K-ions insertion/extraction are presented in Figure 3C,D. The peaks located at 25.2°, 35.4°, and 36.2° belong to $K_{0.7}Fe_{0.5}Mn_{0.5}O_2$, and these three peaks stay throughout the electrochemical processes. Upon depotassiation/potassiation processes, three changes in the XRD patterns can be noticed. First, no change is observed for the peak located at 25.2° during the early charging process, and when the voltage changes from
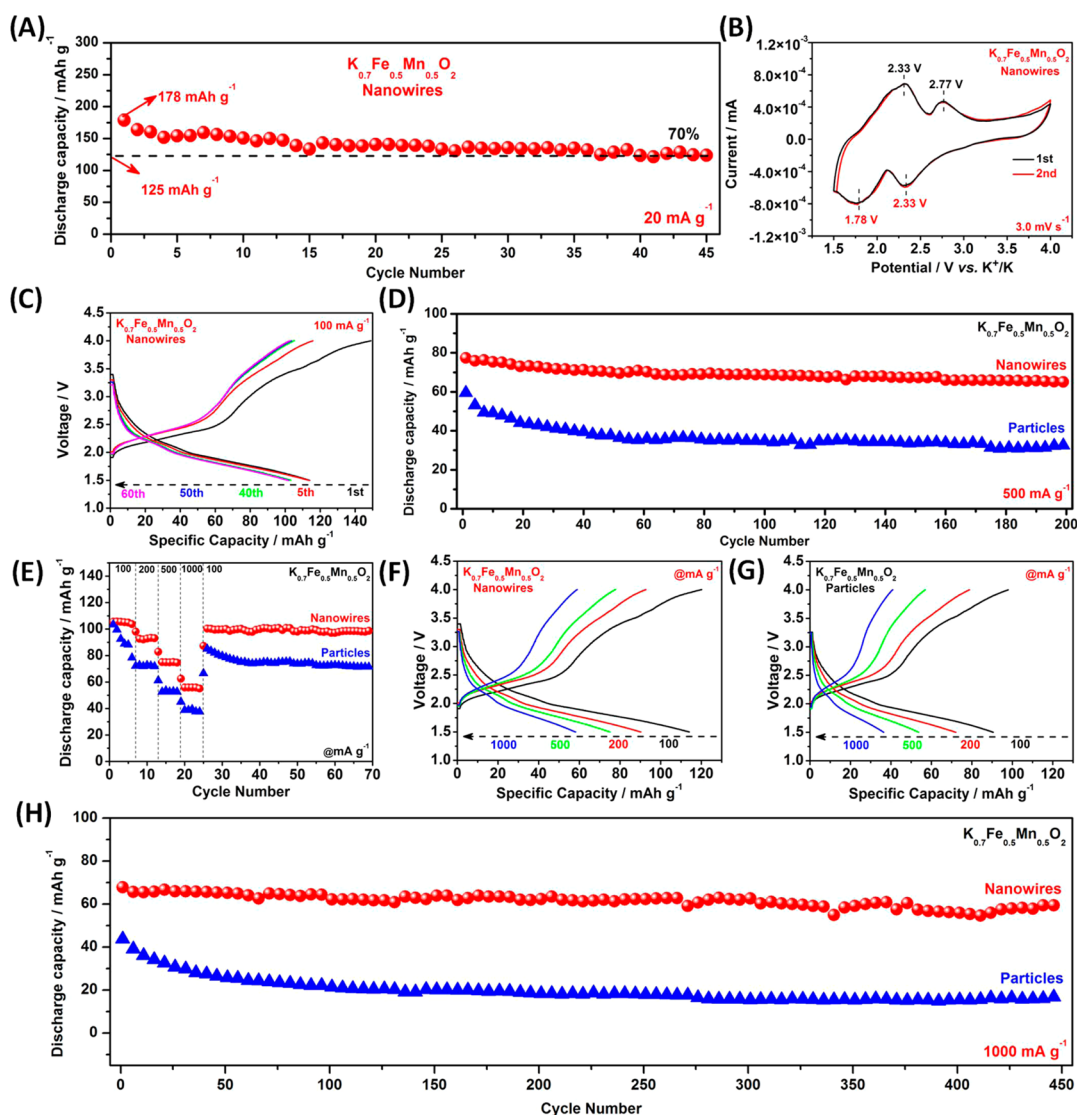
Figure 4. Characterization and comparison of electrochemical performance for interconnected $K_{0.7}Fe_{0.5}Mn_{0.5}O_2$ nanowires and $K_{0.7}Fe_{0.5}Mn_{0.5}O_2$ particles in KIBs. (A) Cyclic performance tested at 20 mA g^{-1}. (B) Cyclic voltammograms. (C) Depotassiation/potassiation curves tested at 100 mA g^{-1}. (D) Cycling performance measured at 500 mA g^{-1}. (E) Rate performance. (F,G) Depotassiation/potassiation curves at various current densities. (H) Long-life cycling performance.

3.27 to 3.7 V the peak weakened and gradually disappeared. Second, one new peak appears and is finally fixed at 26.0° when charged to 4.0 V. Third, this trend is reversed during the first potassiation stage, indicting a reversible expansion contraction.[47,48] Similar behavior also appeared in the second cycle. The peak position of $K_{0.7}Fe_{0.5}Mn_{0.5}O_2$ is restored to that of the original location at the second cycle, but the peak shape becomes broadened. The peak shift shows a small variation, which is owing to the insertion/extraction of K-ions.[49,50] The other two peaks (35.4° and 36.2°) exhibit a minor shift to low angle at the end of depotassiation then return to their original position during the subsequent potassiation process, manifesting a highly stable framework structure of interconnected $K_{0.7}Fe_{0.5}Mn_{0.5}O_2$ nanowires during electrochemical processes.[18,51] Moreover, all the peaks are stably preserved or highly reversible in the following depotassiation/potassiation processes apart from changes in peak intensities, confirming that $K_{0.7}Fe_{0.5}Mn_{0.5}O_2$ can provide a stable crystal framework.[33,52]

On the basis of the in situ XRD analysis, we demonstrate that $K_{0.7}Fe_{0.5}Mn_{0.5}O_2$ can provide a stable crystal framework during the K-ions insertion/extraction. As a consequence, the interconnected $K_{0.7}Fe_{0.5}Mn_{0.5}O_2$ nanowires manifest excellent potassium storage performance, when measured as a cathode in KIBs. First, a high initial discharge capacity of 178 mAh g^{-1} is achieved, when tested at 20 mA g^{-1}. Moreover, a discharge capacity of 125 mAh g^{-1} is retained after 45 cycles, corresponding to a considerable capacity retention of ∼70% (Figure 4A). The cyclic voltammetry (CV) curves for interconnected $K_{0.7}Fe_{0.5}Mn_{0.5}O_2$ nanowires show that two oxidation peaks are located at 2.33 and 2.77 V in the first anodic process (Figure 4B). In the following cathodic process, the corresponding two reduction peaks appeared (2.33 and 1.78 V). Apparently, the first two CV curves share the same characteristics, indicating the same reaction mechanism and high reversibility of K-ions insertion/extraction.[53,54]

In general, the interconnected $K_{0.7}Fe_{0.5}Mn_{0.5}O_2$ nanowires manifest better potassium storage performance than those of $K_{0.7}Fe_{0.5}Mn_{0.5}O_2$ particles. The interconnected $K_{0.7}Fe_{0.5}Mn_{0.5}O_2$
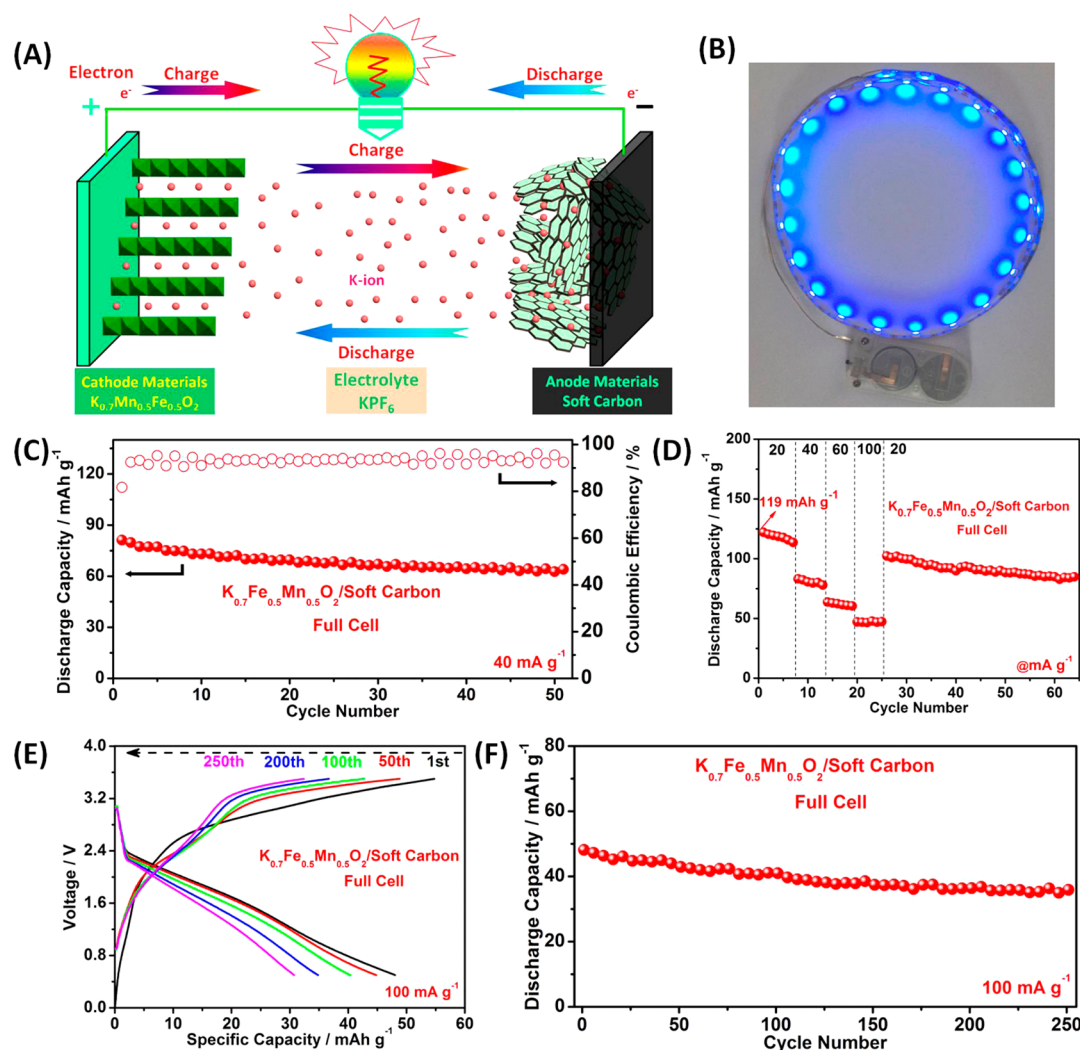
Figure 5. Schematic illustration and electrochemical performance of the full cell based on interconnected $K_{0.7}Fe_{0.5}Mn_{0.5}O_2$ nanowires/soft carbon. (A) Schematic illustration of the K-ion full battery. (B) The lighted LED belts driven by the K-ion full batteries. (C) Cyclic performance and the corresponding Coulombic efficiency at 40 mA g^{-1}. (D) Rate performance. (E) Depotassiation/potassiation curves. (F) Cycling performance at 100 mA g^{-1}.

nanowires exhibit a considerable initial discharge capacity of 114 mAh g^{-1}, maintaining a capacity of 101 mAh g^{-1} after 60 cycles (capacity retention rate is 89%) at 100 mA g^{-1} (Figure S7A). The initial Coulombic efficiency is 87.6%. It stabilized around 98.0% in following cycles, which is substantially greater than that of $K_{0.7}Fe_{0.5}Mn_{0.5}O_2$ particles (Figure S7B). The $K_{0.7}Fe_{0.5}Mn_{0.5}O_2$ particles with an initial capacity of 100 mAh g^{-1} under the same condition, retaining 78 mAh g^{-1} after 60 cycles. Two small potassiation plateaus are observed at around 1.8 and 2.3 V. Also, the depotassiation/potassiation curves of interconnected $K_{0.7}Fe_{0.5}Mn_{0.5}O_2$ nanowires are also similar in following cycles, manifesting excellent cycling stability (Figure 4C). Accordingly, the $K_{0.7}Fe_{0.5}Mn_{0.5}O_2$ particles show a low capacity and poor cycling stability (Figure S8). When tested at 200 mA g^{-1}, the interconnected $K_{0.7}Fe_{0.5}Mn_{0.5}O_2$ nanowires show the initial capacity of 94 mAh g^{-1}, and 96% initial discharge capacity is retained after 45 cycles (Figure S9). By contrast, the capacity of the $K_{0.7}Fe_{0.5}Mn_{0.5}O_2$ particles decays to below 42 mAh g^{-1} in 45 cycles. The interconnected $K_{0.7}Fe_{0.5}Mn_{0.5}O_2$ nanowires can be charged/discharged at 500 mA g^{-1} for 200 cycles with a high capacity retention of 85%

(Figure 4D). However, $K_{0.7}Fe_{0.5}Mn_{0.5}O_2$ particles exhibit a low capacity retention (∼55%) after 200 cycles.

The interconnected $K_{0.7}Fe_{0.5}Mn_{0.5}O_2$ nanowires exhibit a higher capacity and better rate recovery than that of $K_{0.7}Fe_{0.5}Mn_{0.5}O_2$ particles when tested in rate performance measurements, demonstrating a prominent rate performance (Figure 4E−G). When the current density is returned from 1000 to 100 mA g^{-1}, ∼95% of the initial capacity is retained for the interconnected $K_{0.7}Fe_{0.5}Mn_{0.5}O_2$ nanowires, while only ∼82% of the initial capacity is recovered for $K_{0.7}Fe_{0.5}Mn_{0.5}O_2$ particles. The most appealing property of interconnected $K_{0.7}Fe_{0.5}Mn_{0.5}O_2$ nanowires is its outstanding cycling stability at high current densities. When tested at 1000 mA g^{-1}, ∼92% of the capacity retention is obtained after 200 cycles and ∼87% of the capacity retention is achieved after 450 cycles (Figure 4H). By contrast, only ∼36% of the capacity retention is achieved for the $K_{0.7}Fe_{0.5}Mn_{0.5}O_2$ particles after 450 cycles. To the best of our knowledge, our interconnected $K_{0.7}Fe_{0.5}Mn_{0.5}O_2$ nanowires cathode materials exhibit the best electrochemical performance among KIB cathodes in terms of reversible discharge capacity, cycling stability and rate capability (Table S2).

On the basis of the Randles-Sevick equation, the apparent diffusion coefficients of K-ions into $K_{0.7}Fe_{0.5}Mn_{0.5}O_2$ are calculated.[55,56] From the slope value of the fitting line (Figure S10A,C), the apparent diffusion coefficients (D) of the interconnected $K_{0.7}Fe_{0.5}Mn_{0.5}O_2$ nanowires is determined to be 5.6×10^{-9} cm^2 s^{-1} (Figure S10B), which is much higher than that of $K_{0.7}Fe_{0.5}Mn_{0.5}O_2$ particles (3.0×10^{-10} cm^2 s^{-1}) (Figure S10D). The Nyquist plots test results indicate that interconnected $K_{0.7}Fe_{0.5}Mn_{0.5}O_2$ nanowires show lower charge transfer resistance (R_{ct}) before depotassiation/potassiation and after 60 cycles, compared with $K_{0.7}Fe_{0.5}Mn_{0.5}O_2$ particles, indicating a fast electronic mobility (Figure S11). These above results indicate that the constructed interconnected $K_{0.7}Fe_{0.5}Mn_{0.5}O_2$ nanowires can provide fast ion and electron transport channels, leading to a better rate performance than $K_{0.7}Fe_{0.5}Mn_{0.5}O_2$ particles.[56−58] The structural stability of the interconnected $K_{0.7}Fe_{0.5}Mn_{0.5}O_2$ nanowires and $K_{0.7}Fe_{0.5}Mn_{0.5}O_2$ particles are further studied by ex situ SEM (Figure S12). The results demonstrate that the interconnected $K_{0.7}Fe_{0.5}Mn_{0.5}O_2$ nanowires exhibit better structural stability than $K_{0.7}Fe_{0.5}Mn_{0.5}O_2$ particles, resulting in the significant difference in their cycling stability.[32,34,52]

The K-ion full batteries based on interconnected $K_{0.7}Fe_{0.5}Mn_{0.5}O_2$ nanowires, soft carbon, and electrolyte (0.8 M KPF$_6$) were also fabricated. The detailed electrochemical behaviors are shown in Figure 5. Before the full cell assembly, the characterizations of soft carbon are also presented in Figures S13 and S14. The mass loading of the anode is 1.2 times larger than that of the cathode. Figure 5A displays the schematic of the K-ion conduction between $K_{0.7}Fe_{0.5}Mn_{0.5}O_2$ and soft carbon during the K-ion insertion/extraction. The negative electrode is a soft carbon that holds K-ions in its framework, whereas the positive electrode is $K_{0.7}Fe_{0.5}Mn_{0.5}O_2$ with a layered skeleton. Both electrode materials are capable of reversibly insert/extract K-ions from their respective skeleton structure.[11] During the potassiation process, K-ions are extracted from the $K_{0.7}Fe_{0.5}Mn_{0.5}O_2$ and inserted into the soft carbon. The process is reversed during depotassiation. The corresponding lighted LED belts indicate that our full cell can normally work after being fully charged (Figure 5B). As shown in Figure 5C, the full cell delivers a considerable discharge capacity of 82 mAh g^{-1} at 40 mA g^{-1} (based on the mass of the cathode), and the capacity retention rate is ∼90% after 50 cycles. A high initial Coulombic efficiency of ∼92% is achieved in the first cycle (the soft carbon was prepotassiated). As the current density increases from 20 to 40, 60, and 100 mA g^{-1}, the full cell shows an average capacity of 119 (corresponding to the insertion/extraction of ∼0.57 K-ions per formula), 82, 62, and 48 mAh g^{-1}, respectively (Figure 5D). The corresponding depotassiation/potassiation curves from 20 to 100 mA g^{-1} are shown in Figure S15. Significantly, when the rate is returned to 20 mA g^{-1}, the reversible capacity can be recovered to 102 mAh g^{-1}, corresponding to a capacity retention of ∼86%. Notably, when tested at 100 mA g^{-1}, ∼76% of the initial capacity is retained after 250 cycles (Figure 5F), manifesting considerable long-term cycling stability in K-ion full batteries.

The remarkable potassium storage performance of the interconnected $K_{0.7}Fe_{0.5}Mn_{0.5}O_2$ nanowires is attributed to their unique crystal structure and one-dimensional framework. First, the $K_{0.7}Fe_{0.5}Mn_{0.5}O_2$ possesses a highly stable framework (Figures 3C and S12), which is conducive to the cycling stability. Second, the interconnected $K_{0.7}Fe_{0.5}Mn_{0.5}O_2$ nanowires possess aboundant pores (Figures 2F and S6), resulting in

high rate performance. Third, the carbon framework of interconnected nanowires can improve the conductivity and offer three-dimensional continuous electron transport pathways (Figures 1 and 2C). By combining all above advantages, the interconnected $K_{0.7}Fe_{0.5}Mn_{0.5}O_2$ nanowires exhibit impressive electrochemical potassium storage performance with exceptional capacity and excellent cycling stability in K-ion full batteries.

In summary, we have demonstrated that $K_{0.7}Fe_{0.5}Mn_{0.5}O_2$ is a promising candidate for high capacity K-ion full batteries. The full cell shows a capacity of 119 mAh g^{-1} at a current density of 20 mA g^{-1}, corresponding to the insertion/extraction of ∼0.57 K-ions per formula. Besides, on the basis of in situ XRD analysis, we confirm that interconnected $K_{0.7}Fe_{0.5}Mn_{0.5}O_2$ nanowires are featured with stable layered skeleton structure and exhibit high reversibility during depotassiation/potassiation processes. Combined with ion diffusion calculation, interconnected $K_{0.7}Fe_{0.5}Mn_{0.5}O_2$ nanowires are demonstrated to possess fast K-ion diffusion rate compared to that of $K_{0.7}Fe_{0.5}Mn_{0.5}O_2$ particles. Consequently, the interconnected $K_{0.7}Fe_{0.5}Mn_{0.5}O_2$ nanowires exhibit high discharge capacity and excellent cycling stability when used as a cathode in K-ion full batteries. Our work proves that designing and constructing one-dimensional nanomaterials with a stable structure is an effective approach to improve the cycling stability for K-ion full batteries. Moreover, our work may also open up a new direction in large-scale energy storage systems.

■ ASSOCIATED CONTENT

Ⓢ Supporting Information

The Supporting Information is available free of charge on the ACS Publications website at DOI: 10.1021/acs.nano-lett.6b04611.

> Additional characterization results, including experiments section, XRD, ICP, TG, Raman, BET, cycling perform-ance, CV, EIS data, and SEM images (PDF)

■ AUTHOR INFORMATION

Corresponding Authors

*E-mail: niuchaojiang11@whut.edu.cn.
*E-mail: mlq518@whut.edu.cn.

ORCID Ⓘ

Liqiang Mai: 0000-0003-4259-7725

Author Contributions

L.Q.M. and X.P.W. designed the experiments, analyzed the results, and wrote the manuscript. X.P.W. performed the experiments and analyzed the results. All authors commented on the manuscript.

Notes

The authors declare no competing financial interest.

■ ACKNOWLEDGMENTS

Center for Materials Research and Analysis from Wuhan University of Technology.

■ REFERENCES

(1) Palomares, V.; Serras, P.; Villaluenga, I.; Hueso, K. B.; González, J. C.; Rojo, T. *Energy Environ. Sci.* **2012**, *5*, 5884−5901.

(2) Pan, H. L.; Hu, Y. S.; Chen, L. Q. *Energy Environ. Sci.* **2013**, *6*, 2338−2360.

(3) Slater, M. D.; Kim, D.; Lee, E.; Johnson, C. S. *Adv. Funct. Mater.* **2013**, *23*, 947−958.

(4) Peters, J.; Buchholz, D.; Passerini, S.; Weil, M. *Energy Environ. Sci.* **2016**, *9*, 1744−1751.

(5) Soloveichik, G. L. *Annu. Rev. Chem. Biomol. Eng.* **2011**, *2*, 503−527.

(6) Divya, K. C.; Østergaard, J. *Electr. Power Syst. Res.* **2009**, *79*, 511−520.

(7) Chen, H. S.; Cong, T. N.; Yang, W.; Tan, C. Q.; Li, Y. L.; Ding, Y. L. *Prog. Nat. Sci.* **2009**, *19*, 291−312.

(8) Ibrahim, H.; Ilinca, A.; Perron, J. *Renewable Sustainable Energy Rev.* **2008**, *12*, 1221−1250.

(9) Choi, J. W.; Aurbach, D. *Nat. Rev. Mater.* **2016**, *1*, 16013.

(10) Yang, Z. G.; Zhang, J. L.; Kintner-Meyer, M. C. W.; Lu, X. C.; Choi, D.; Lemmon, J. P.; Liu, J. *Chem. Rev.* **2011**, *111*, 3577−3613.

(11) Dunn, B.; Kamath, H.; Tarascon, J. M. *Science* **2011**, *334*, 928−935.

(12) Armand, M.; Tarascon, J. M. *Nature* **2008**, *451*, 652−657.

(13) Kim, H.; Park, C. S.; Choi, J. W.; Jung, Y. *Angew. Chem., Int. Ed.* **2016**, *55*, 6662−6666.

(14) Xu, C. J.; Li, B. H.; Du, H. D.; Kang, F. Y. *Angew. Chem., Int. Ed.* **2012**, *51*, 933−935.

(15) Pan, H. L.; Shao, Y. Y.; Yan, P. F.; Cheng, Y. W.; Han, K. S.; Nie, Z. M.; Wang, C. M.; Yang, J. H.; Li, X. L.; Bhattacharya, P.; Mueller, K. T.; Liu, J. *Nat. Energy* **2016**, *1*, 16039.

(16) Kundu, D.; Talaie, E.; Duffort, V.; Nazar, L. F. *Angew. Chem., Int. Ed.* **2015**, *54*, 3431−3448.

(17) Jian, Z. L.; Luo, W.; Ji, X. L. *J. Am. Chem. Soc.* **2015**, *137*, 11566−11569.

(18) Schuppert, N. D.; Mukherjee, S.; Bates, A. M.; Son, E. J.; Choi, M. J.; Park, S. *J. Power Sources* **2016**, *316*, 160−169.

(19) Komaba, S.; Hasegawa, T.; Dahbi, M.; Kubota, K. *Electrochem. Commun.* **2015**, *60*, 172−175.

(20) Wessells, C. D.; Peddada, S. V.; Huggins, R. A.; Cui, Y. *Nano Lett.* **2011**, *11*, 5421−5425.

(21) Pal, D.; Abdi, S. H.; Shukla, M. *J. Mater. Sci.: Mater. Electron.* **2015**, *26*, 6647.

(22) Padigi, P.; Thiebes, J.; Swan, M.; Goncher, G.; Evans, D.; Solanki, R. *Electrochim. Acta* **2015**, *166*, 32−39.

(23) Xing, Z. Y.; Qi, Y. T.; Jian, Z. L.; Ji, X. L. *ACS Appl. Mater. Interfaces* **2016**, DOI: 10.1021/acsami.6b06767.

(24) Share, K.; Cohn, A. P.; Carter, R.; Rogers, B.; Pint, C. L. *ACS Nano* **2016**, *10*, 9738−9744.

(25) Vaalma, C.; Giffin, G. A.; Buchholz, D.; Passerini, S. *J. Electrochem. Soc.* **2016**, *163*, A1295−A1299.

(26) Jian, Z. L.; Liang, Y. L.; Rodríguez-Pérez, I. A.; Yao, Y.; Ji, X. L. *Electrochem. Commun.* **2016**, *71*, 5−8.

(27) Zhao, Q.; Wang, J. B.; Lu, Y.; Li, Y. X.; Liang, G. X.; Chen, J. *Angew. Chem.* **2016**, *128*, 12716−12720.

(28) Chen, Y.; Luo, W.; Carter, M.; Zhou, L. H.; Dai, J. Q.; Fu, K.; Lacey, S.; Li, T.; Wan, J. Y.; Han, X. G.; Bao, Y. P.; Hu, L. P. *Nano Energy* **2015**, *18*, 205−211.

(29) Yu, G. H.; Cao, A. Y.; Lieber, C. M. *Nat. Nanotechnol.* **2007**, *2*, 372−377.

(30) Niu, C. J.; Meng, J. S.; Wang, X. P.; Han, C. H.; Yan, M. Y.; Zhao, K. N.; Xu, X. M.; Ren, W. H.; Zhao, Y. L.; Xu, L.; Zhang, Q. J.; Zhao, D. Y.; Mai, L. Q. *Nat. Commun.* **2015**, *6*, 7402.

(31) Duan, X. F.; Lieber, C. M. *Nano Res.* **2015**, *8*, 1−22.

(32) Yao, J.; Yan, H.; Lieber, C. M. *Nat. Nanotechnol.* **2013**, *8*, 329−335.

(33) Cao, Y.; Xiao, L.; Sushko, M. L.; Wang, W.; Schwenzer, B.; Xiao, J.; Nie, Z. M.; Saraf, L. V.; Yang, Z. G.; Liu, J. *Nano Lett.* **2012**, *12*, 3783−3787.

(34) Wang, X. P.; Niu, C. J.; Meng, J. S.; Hu, P.; Xu, X. M.; Wei, X. J.; Zhou, L.; Zhao, K. N.; Luo, W.; Yan, M. Y.; Mai, L. Q. *Adv. Energy Mater.* **2015**, *5*, 1500716.

(35) Mai, L. Q.; Tian, X. C.; Xu, X.; Chang, L.; Xu, L. *Chem. Rev.* **2014**, *114*, 11828−11862.

(36) Lieber, C. M. *MRS Bull.* **2011**, *36*, 1052−1063.

(37) Cao, Y.; Xiao, L.; Wang, W.; Choi, D.; Nie, Z. M.; Yu, J. G.; Saraf, L. V.; Yang, Z. G.; Liu, J. *Adv. Mater.* **2011**, *23*, 3155−3160.

(38) Hu, Y. J.; Kuemmeth, F.; Lieber, C. M.; Marcus, C. M. *Nat. Nanotechnol.* **2011**, *7*, 47−50.

(39) Liu, Y. C.; Zhang, N.; Yu, C. M.; Jiao, L. F.; Chen, J. *Nano Lett.* **2016**, *16*, 3321−3328.

(40) Kalluri, S.; Seng, K. H.; Pang, W. K.; Guo, Z. P.; Chen, Z. X.; Liu, H. K.; Dou, S. X. *ACS Appl. Mater. Interfaces* **2014**, *6*, 8953−8958.

(41) Zhang, B.; Kang, F. Y.; Tarascon, J.-M.; Kim, J.-K. *Prog. Mater. Sci.* **2016**, *76*, 319−380.

(42) Li, W. H.; Zeng, L. C.; Wu, Y.; Yu, Y. *Sci. China Mater.* **2016**, *59*, 287−321.

(43) Yu, Y.; Lin, G.; Zhu, C. B.; van Aken, P. A.; Maier, J. *J. Am. Chem. Soc.* **2009**, *131*, 15984−15985.

(44) Wu, H.; Chan, G.; Choi, J. W.; Ryu, I.; Yao, Y.; McDowell, M. T.; Lee, S. W.; Jackson, A.; Yang, Y.; Hu, L. B.; Cui, Y. *Nat. Nanotechnol.* **2012**, *7*, 310−315.

(45) Jänes, A.; Thomberg, T.; Kurig, H.; Lust, E. *Carbon* **2009**, *47*, 23−29.

(46) Hu, P.; Yan, M. Y.; Wang, X. P.; Han, C. H.; He, L.; Wei, X. J.; Niu, C. J.; Zhao, K. N.; Tian, X. C.; Wei, Q. L.; Li, Z. J.; Mai, L. Q. *Nano Lett.* **2016**, *16*, 1523−1529.

(47) Zhao, Y. L.; Feng, J. G.; Liu, X.; Wang, F. C.; Wang, L. F.; Shi, C. W.; Huang, L.; Feng, X.; Chen, X. Y.; Xu, L.; Yan, M. Y.; Zhang, Q. J.; Bai, X. D.; Wu, H. G.; Mai, L. Q. *Nat. Commun.* **2014**, *5*, 4565.

(48) Xu, S. Y.; Wang, Y. S.; Ben, L. B.; Lyu, Y. C.; Song, N. N.; Yang, Z. Z.; Li, Y. M.; Mu, L. Q.; Yang, H.-T.; Gu, L.; Hu, Y.-S.; Li, H.; Cheng, Z.-H.; Chen, L. Q.; Huang, X. J. *Adv. Energy Mater.* **2015**, *5*, 1501156.

(49) Wang, Y. S.; Liu, J.; Lee, B.; Qiao, R. M.; Yang, Z. Z.; Xu, S. Y.; Yu, X. Q.; Gu, L.; Hu, Y.-S.; Yang, W. L.; Kang, K.; Yang, X.-Q.; Chen, L. Q.; Huang, X. J. *Nat. Commun.* **2015**, *6*, 6401.

(50) Liu, H.; Strobridge, F. C.; Borkiewicz, O. J.; Wiaderek, K. M.; Chapman, K. M.; Chupas, P. J.; Grey, C. P. *Science* **2014**, *344*, 1252817.

(51) Wang, Y. S.; Xiao, R. J.; Hu, Y.-S.; Avdeev, M.; Chen, L. Q. *Nat. Commun.* **2015**, *6*, 6954.

(52) Li, Y. M.; Yang, Z. Z.; Xu, S. Y.; Mu, L. Q.; Gu, L.; Hu, Y. S.; Li, H.; Chen, L. Q. *Adv. Sci.* **2015**, *2*, 1500031.

(53) Xie, Q. S.; Ma, Y. T.; Wang, X. P.; Zeng, D. Q.; Wang, L. S.; Mai, L. Q.; Peng, D.-L. *ACS Nano* **2016**, *10*, 1283−1291.

(54) Fedotov, S. S.; Khasanova, N. R.; Samarin, A. S.; Drozhzhin, O. A.; Batuk, D.; Karakulina, O. M.; Hadermann, J.; Abakumov, A. M.; Antipov, E. V. *Chem. Mater.* **2016**, *28*, 411−415.

(55) Levine, L. E.; Larson, B. C.; Yang, W.; Kassner, M. E.; Tischler, J. Z.; Reyes, M. A. D.; Fields, R. J.; Liu, W. J. *Nat. Mater.* **2006**, *5*, 619−622.

(56) Jung, H.-G.; Hassoun, J.; Park, J.-B.; Sun, Y.-K.; Scrosati, B. *Nat. Chem.* **2012**, *4*, 579−585.

(57) Wang, Y. X.; Yang, J. P.; Chou, S. L.; Liu, H. K.; Zhang, W. X.; Zhao, D. Y.; Dou, S. X. *Nat. Commun.* **2015**, *6*, 8689.

(58) Qi, X. G.; Wang, Y. S.; Jiang, L. W.; Mu, L. Q.; Zhao, C. L.; Liu, L. L.; Hu, Y.-S.; Chen, L. Q.; Huang, X. J. *Part. Part. Syst. Char.* **2015**, *1*, 1500129.